

# Three-Dimensional Robotic Manipulation and Transport of Micro-Scale Objects by a Magnetically Driven Capillary Micro-Gripper

Joshua Giltinan, Eric Diller, Cagil Mayda, and Metin Sitti

**Abstract**—One major challenge for untethered micro-scale mobile robotics is the manipulation of external objects in the robot's three-dimensional (3D) work environment. Here, we present a method to use the capillary force at a solid-liquid-gas interface to reversibly attach objects to a mobile magnetic microrobot. This is accomplished by the addition of a cavity in the hydrophobic microrobot, in which an air bubble is captured when the microrobot is placed in a water environment. The extension of the air bubble from the cavity is adjusted dynamically by controlling the pressure of the workspace environment. A peak switching ratio between the maximum and minimum gripping forces of 14:1 is shown for controlled attachment/detachment experiments, which allows for reliable pick-and-place operation. This work introduces an analytical capillary adhesion model and demonstrates control of the bubble size for pick-and-place gripping. A proof-of-concept demonstration of 3D manipulation in a fluidic environment shows the potential of capillary gripping for future use in confined environments such as inside microfluidic devices for transportation or assembly of hydrophobic objects.

## I. INTRODUCTION

In recent years, great strides have been made in power delivery and control of untethered micro-scale robotics. The current designs in literature, including electrostatic [1], electromagnetic [2], thermal [3], and bacteria-propelled systems [4], [5], have demonstrated wireless motion control of individual and groups of mobile microrobots. A major challenge for microrobots is the manipulation of sub-millimeter size objects, which is envisioned to be critical for micro-assembly tasks and minimally-invasive surgery [6].

Magnetic microrobots are of particular interest to researchers as magnetic fields can be used for remote actuation at long range and are capable of applying relatively large forces and torques. Actuation has been demonstrated in a variety of environments, including liquid and air, and fluid-based actuation has been demonstrated in both 2D and 3D [7].

Previously, researchers have shown manipulation of micro-objects in 2D using contact and non-contact fluid-based manipulation, with control methods that work well constrained to a planar surface, yet yield some difficulty in 3D [8], [9], [10]. Tottori et al. showed the 3D manipulation of 6  $\mu\text{m}$  diameter microparticles by 35  $\mu\text{m}$  long magnetic microrobots which swim with a helical flagellum and use a cup to hold the micro-object [11]. Kwon et al. demonstrated the use of an ultrasonic transducer to control the oscillation of an air bubble attached to a microrobot in a fluid medium. The oscil-

J. Giltinan, E. Diller, and M. Sitti\* are with the Department of Mechanical Engineering, Carnegie Mellon University, Pittsburgh, PA 15213, USA. E. Diller is now with the Department of Mechanical and Industrial Engineering, University of Toronto, Toronto, M5S3G8, Canada. C. Mayda is with the Department of Engineering and Natural Sciences, Sabanci University, Istanbul 34956, Turkey. \*sitti@cmu.edu

lation of the air bubble near the bubble's resonant frequency induced fluid flow used to trap objects, and the generated force had a measured output of 50 nN [12]. As these works either constrain the geometry of the object or have a low actuating force to weight ratio, the untethered pick-and-place manipulation of small objects in 3D with arbitrary geometries remains an unsolved challenge in microrobotics.

Tethered gripping of micro scale objects has been well studied. In air, MEMS- and vacuum-based grippers have been shown to reliably and precisely pick-and-place objects [13]. Water as an operating environment is of particular interest for medical applications as many biological fluids are comprised of water, and retain similar fluid properties. In water, López-Walle et al. use a Peltier element to cool a tethered end-effector, creating ice in the water. This ice traps micro-objects, and the end-effector is able to melt the ice to release the object after manipulation [14]. However, tethered methods such as these cannot be easily converted into micro-scale mobile systems.

Capillary and surface forces have been demonstrated for the manipulation of micro-scale objects with minimal damage and with a high level of controllability. Many of these works use water as the bridging medium and operate in air [15]. A capillary gripper could take advantage of hydrophobic interactions and would not be dependent on the microrobot resting on a surface, being advantageous for 3D motion.

This work introduces a capillary gripping mechanism to previously-developed magnetic micro-robots capable of 5-DOF motion in fluid. This method relies on surface forces at a solid-liquid-gas interface to grab objects of an arbitrary shape with adhesion on the order of five to ten microneutons. As the gripping principle is not dependent on the microrobot motion strategy, the method presented can be used in other microrobotic systems.

A gas bubble is attached to the microrobot, and the bubble uses surface forces to attach to the object to be manipulated. The volume of the trapped air bubble can be modulated by changing the ambient pressure of the micro-robot's environment in a remote manner. This allows for control of the adhesive force exerted on the object, allowing for controllable pick-and-place gripping of arbitrarily shaped objects. This paper presents the concept of manipulation using a bubble, an analytical model and characterization of attachment forces, the system used to actuate the gripping microrobots, and a demonstration of micro-object transport in 3D.

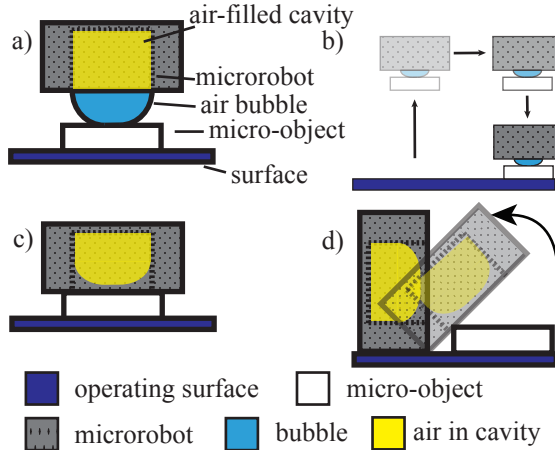


Fig. 1: Manipulation of a micro-sized object by a magnetic microrobot using a capillary gripper. (a) The microrobot, with bubble extended, approaches and attaches to the object. The dashed lines show the cross section depicting the air cavity inside the microrobot. It is possible for the microrobot to position itself onto the object in 2D or 3D. (b) The microrobot, attached to the object by a capillary bridge, moves in 3D and places the object on a surface. (c) The bubble retracts into the microrobot, breaking contact with the object. (d) With attachment force minimized, the microrobot peels/rolls off of the object, leaving it on the surface.

## II. CAPILLARY GRIPPING CONCEPT

When a polyurethane/NdFeB composite microrobot is placed in a water, the hydrophobic surface will capture air bubbles due to nucleation sites that occur as a result of the surface roughness of the polyurethane/NdFeB material [16]. A molded cavity in a microrobot will repeatably capture a proportionally sized air bubble at a specific location. In a water environment, hydrophobic objects will prefer to be in contact with the air bubble in order to minimize their surface energy. In kind, the air bubble will minimize its surface energy by being contact with other objects. The air bubble then acts as a capillary bridge between the microrobot cavity and the micro-object. Through this bridge the microrobot can exert forces on the object to move it in the microrobot's workspace. However, the attachment force between the micro-object and bubble must be greater than the attractive forces between the micro-object and the work environment; this work assumes this is always true. The releasing mechanism is thus a result of the bubble breaking attachment with the micro-object. It is also assumed that the total force attaching the bubble to the microrobot is greater than the total force attracting the bubble to the micro-object, thus when an external influence causes the bubble volume to decrease, it is assumed the bubble retracts into the cavity of the microrobot. The height of the bubble extending from the microrobot,  $h$ , decreases until all contact with the micro-object is broken, as shown in Fig. 1. We generalize this condition to be  $h < 0$ , as we are unable to see small and negative bubble heights.

The air bubble extension is manipulated by controlling the pressure in the microrobot workspace. This is done via an air-tight chamber in which the microrobot work environment is placed. The internal relative pressure of the chamber, which is monitored by a pressure gauge, is modulated by a pump connected to the chamber by a tube. Alternative

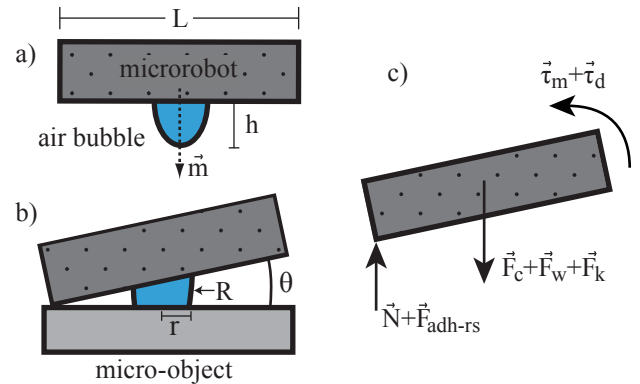


Fig. 2: Forces acting on a microrobot (a) Relevant dimensions and microrobot moment  $\vec{m}$ . (b) Measured parameters during the adhesion measurement. (c) Free body diagram of the microrobot during these tests. The adhesion, weight, and the spring force of the bubble are approximated to act on the center of the microrobot. The normal force and adhesion between the microrobot and substrate act on the pivot point of the microrobot.

bubble manipulation methods, such as controlling the local temperature of the bubble volume by remote inductive magnetic heating, could be used to avoid the constraints of a pressurized chamber, but are beyond the scope of this work.

### A. Magnetic Forces and Torques

Magnetic forces and torques can be induced by a set of electromagnetic coils surrounding the workspace. These forces and torques can be used to directly move the microrobot in space, and has been demonstrated for 2D motion on a surface or for 3D motion in fluid environments [17]. A magnetic microrobot experiences torques due to the magnetic fields and forces due to the magnetic field gradients. The force  $\vec{F}_m$  exerted on a microrobot with magnetic moment  $\vec{m}$  in a magnetic field  $\vec{B}$ , assuming no electric current is flowing in the workspace, is

$$\vec{F}_m = (\vec{m} \cdot \nabla) \vec{B}, \quad (1)$$

and the magnetic torque  $\vec{\tau}_m$  is given by

$$\vec{\tau}_m = \vec{m} \times \vec{B}. \quad (2)$$

### B. Capillary Force

When the bubble comes into contact with another surface, surface tension and Laplace forces will attach the bubble to the surface. The Laplace force,  $\vec{F}_p$ , is due to the pressure difference between the bubble's internal pressure, and the pressure of the workspace. The surface tension force,  $\vec{F}_{st}$ , arises from the surface tension at the interface between the object, liquid, and bubble. Together, the Laplace and surface tension forces are considered to be the capillary force acting on the object.

To simplify the problem, we assume the microrobot and object are parallel plates with an axisymmetric capillary bridge. For two planar parallel surfaces, the capillary force between them is

$$\vec{F}_c = \vec{F}_{st} + \vec{F}_p = 2\pi r \gamma \sin(\theta_c) + \pi r^2 \Delta P, \quad (3)$$

where  $r$  is the radius of the contact circle between the object and the bubble,  $\theta_c$  is the contact angle of water on the object surface,  $\gamma$  is the surface tension of the solid-liquid-gas interface (72 mN/m for water-air) and  $\Delta P$  is the pressure drop across the bubble interface. This pressure drop is given by Laplace's law as

$$\Delta P = 2\gamma/R, \quad (4)$$

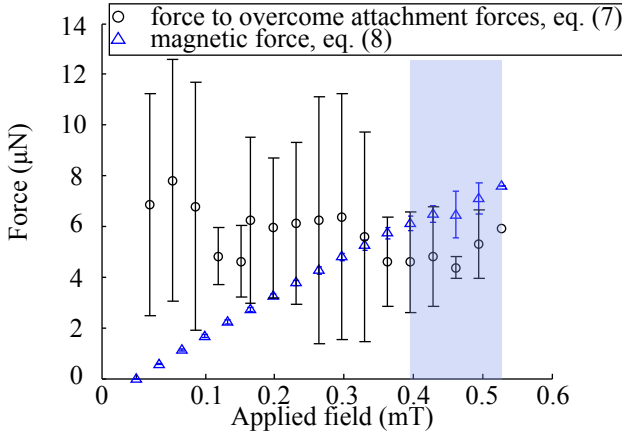


Fig. 3: Comparison of the applied magnetic force, eq. (8) and the magnetic force required for detachment by peeling, eq. (7). The microrobot is observed five times attaching to and peeling from the same surface. There are three samples per data point for  $\vec{B}$  in the range 0–0.165 mT due to the inability to conduct visual measurements in this range for two samples. Microrobot magnetization:  $\vec{m} = 4.4 \mu\text{Am}^2$ .

where  $R$  is the mean radius of curvature of the water-vapor surface [15].

When in contact with an object, the bubble will maintain a non-zero  $h$  above the surface. This is due to a restoring force the bubble exerts on the microrobot, which for small forces can be considered Hookean, and is given by

$$\vec{F}_k = k(h - h_0), \quad (5)$$

where  $h_0$  is the bubble height in absence of an applied force. In experiments,  $h$  is measured from the middle of the bubble cavity directly down to the micro-object, as seen in Fig. 2. The approximated minimum observed height,  $h_0$ , occurs in the absence of an applied magnetic field, but still in the presence of the weight of the microrobot. Attard et al. have shown that the effective spring constant  $k$  of a bubble or droplet experiencing a load by a small particle with radius  $R_p$ , can be approximated as

$$k = 4\pi\gamma \left( \ln \left[ \frac{2\kappa R_0^2}{R_p} \frac{\sin^2(\theta_c)}{(1 + \cos(\theta_c))^2} \right] - \frac{\cos(\theta_c)}{2 + \cos(\theta_c)} \right)^{-1}, \quad (6)$$

where  $\kappa^{-1} \approx 10 \text{ nm}$  is the electric double layer force of decay length and  $R_0$  is the unperturbed radius of curvature, which for small forces  $R_0 \approx R$  [18]. Here,  $R_p$  is approximated by the radius of contact,  $r$ .

### III. ADHESION MEASUREMENTS

The gripping force of a capillary gripping microrobot is characterized by affixing a silicon substrate to the pressure chamber surface and having the microrobot peel off by applying a magnetic torque. First, the microrobot is oriented to have the bubble come in contact with the fixed substrate. Then a magnetic torque is applied to peel the microrobot from the surface, and the capillary force acts as an opposing moment. Figure 2 shows the balance of forces and torques acting on a microrobot used to measure the adhesion of an attached bubble. Assuming the microrobot motion is slow, the fluid drag,  $\tau_d$ , is negligible. Approximating the forces to act on the center of the microrobot, the force required to overcome the capillary force, bubble restoring force, and

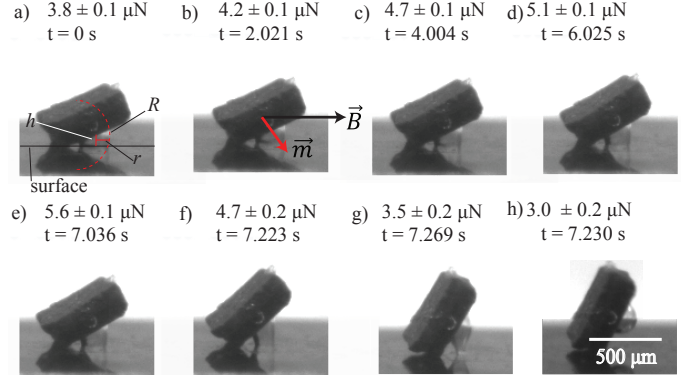


Fig. 4: High speed images of a microrobot with a bubble peeling off a bare silicon substrate. The force due to the applied magnetic torque is given for each frame. The error given is due to a possible  $\pm 2^\circ$  measurement error of the microrobot angle. The time given is referenced to the initial measurement time. An undesired bubble on the side of the microrobot facing the camera is visible. An example of parameters found by analysis is given in a). Here,  $R_2 \approx R_1 = 160 \mu\text{m}$ ,  $h = 85 \mu\text{m}$ , and  $r = 80 \mu\text{m}$  with a measurement error of approximately  $\pm 5 \mu\text{m}$ . The direction of  $\vec{m}$  and  $\vec{B}$  are given in (b).

effective weight  $\vec{F}_w$ , can be solved as

$$\vec{F}_o = \vec{F}_c + \vec{F}_k + \vec{F}_w, \quad (7)$$

In manipulation, the applied forces to the microrobot should be lower than  $\vec{F}_o$  in order to prevent undesired detachment. The capillary and spring forces are obtained using eqs. (3,6) by measuring  $r$ ,  $R$ , and  $h$ . The measurements are obtained by using the ImageJ software suite based on optical images. An example measurement is shown in Fig. 4(a). The mean bubble curvature is estimated by taking the mean of the measured radius of curvature of the meniscus at the greatest separation between the microrobot and the substrate and the measured radius of curvature of the meniscus at the shortest separation.

The force overcoming the capillary bond in this case is the equivalent force at the bubble site due to the induced magnetic torque, which is given by

$$\vec{F}_{mt} = \frac{2}{L} |\vec{m}| |\vec{B}| \sin \theta, \quad (8)$$

where  $\theta$  is the angle between the microrobot and the surface, and  $L$  is the pivot arm length of the microrobot.

Figure 3 compares the applied  $\vec{F}_{mt}$  to  $\vec{F}_o$  for an unretracted bubble on a fixed silicon surface. A relative pressure of approximately  $-24 \text{ kPa}$  is applied to the microrobot workspace to expand the bubble. This pressure is chosen as the resulting large bubble size facilitates the measurement of the capillary force parameters. The applied field is increased by increments of 0.03 mT every two seconds until the microrobot orients with the field and peels the bubble from the surface. Detachment of the microrobot occurred differently for each iteration in the values between 0.4 and 0.53 mT, all occurring when the applied magnetic force is greater than the force required for detachment. This is represented by the shaded region. To calculate eq. (7), the values of  $h$ ,  $R$ , and  $r$  must be determined by analyzing frames of the experiment. Measurement of  $h$ ,  $R$ , and  $r$  yields an error of  $\approx \pm 5 \mu\text{m}$  per variable, and in addition to stochastic variations, results in a large overall error. Error in the applied magnetic force is due to the measurement of the microrobot angle. This shows that the required detachment forces are on the order of 5 to 10

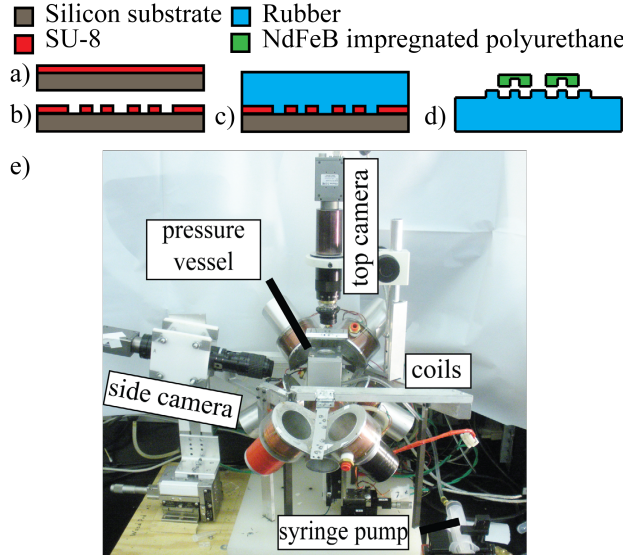


Fig. 5: (a-c) Fabrication of capillary gripping microrobots. The microrobots are fabricated as in previous work [19]. (d) A thick backing layer is left so the microrobot forms a one-sided cavity for bubble capture. (e) Eight coil electromagnet system used for microrobot experiments. The pressure vessel is placed in the center of the workspace and is connected to the syringe pump which controls the pressure.

$\mu\text{N}$ , which are greater than the  $\approx 1 \mu\text{N}$  the electromagnetic coils are able to create through magnetic gradients ( $\vec{F}_m$ ) for a microrobot with a magnetization of  $1 \mu\text{Am}^2$ . The weight of the microrobot and proof of concept micro-object are on the order of  $1 \mu\text{N}$ , thus the attachment force to weight ratio is approximately 10:1.

To demonstrate the bubble deformation as the microrobot is peeled from the surface, a high speed camera (pco.dimax) at 1000 frames per second captured the deformation of the bubble and the resulting microrobot angle,  $\theta$ , for an applied field. The field is increased from 0.23 to 0.36 mT by 0.033 mT every two seconds, and the frame is acquired after the microrobot reaches equilibrium, generally after one second. The bubble curvature,  $R$ , does not change drastically until the increasing angle of the microrobot begins to decrease  $F_{mt}$ . This is shown in Fig. 4 for an applied relative pressure of  $\approx -24 \text{ kPa}$ .

#### IV. SYSTEM DESIGN AND CHARACTERIZATION

##### A. Magnetic and Pressure Actuation

An electromagnetic coil system is used to actuate the microrobots remotely. The system is capable of applying maximum magnetic fields of 27 mT and a spatial gradient of 1 mT/mm. The magnetic coil system used is described in detail by Diller et al. [7] and is shown, with the pressure vessel in the workspace, in Fig. 5(e).

##### B. Pressure Chamber Design

The pressure chamber is made from aluminum with acrylic viewing ports, and flexible PVC tubing connects it to a 30 mL syringe. Pressure is measured by digital meter (ACSI Model 1200). The syringe is mounted to a pump (Braintree Sci BS-8000) for precise manipulation of the bubble height.

##### C. Microrobots

Permanent magnet microrobots are fabricated in a batch process using photolithography and molding techniques similar to Imbabi et al. [20]. Microrobots are composed of

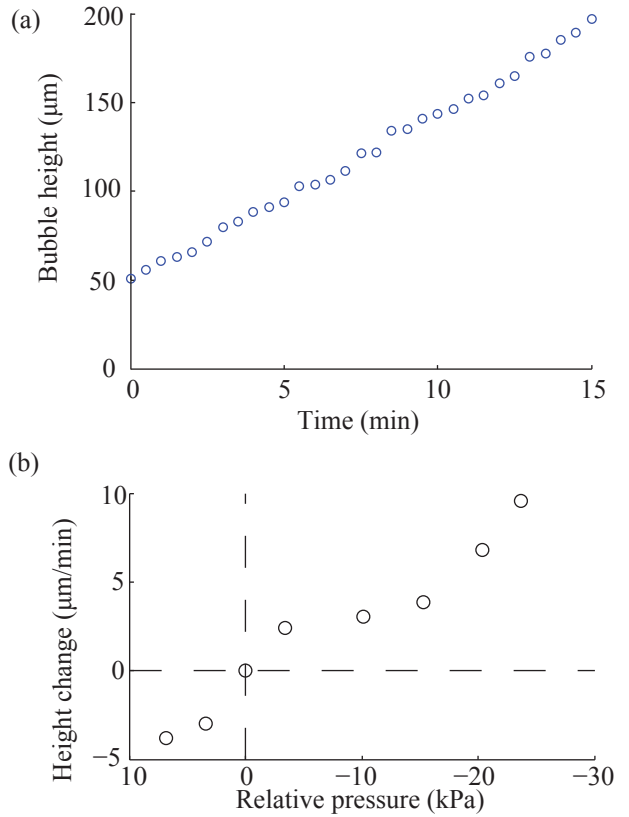


Fig. 6: Characterization of bubble growth rate from gas diffusion from the surrounding water. (a) Change in bubble size vs time for a stabilized relative pressure of  $\approx -24 \text{ kPa}$ . The bubble height starts from an arbitrary  $51 \mu\text{m}$  and over 15 minutes grows to  $197 \mu\text{m}$ . (b) The rate of change of a bubble size for the spectrum of relative pressures investigated and used for the manipulation method. The rates are determined from data sets as illustrated in (a) and are taken as the least squares fit of the data.

neodymium-iron-boron (NdFeB) particles in a polyurethane matrix, with fabrication details given by Diller et al. [19]. To form an asymmetric feature, the microrobot cavity, a special consideration is needed in the molding process. As shown in Fig. 5(d), the cavity is formed by filling the mold with excess material, forming a thick backing layer on the mold. The microrobots are removed from the mold, and excess material is trimmed before the microrobots are magnetized. The magnetization of the microrobot is measured using an alternating field gradient magnetometer.

#### V. DISCUSSION

##### A. Bubble Capture and Height

A bubble is considered successfully captured when the resulting air pocket is relatively flush with the microrobot side ( $h \approx 0$ ) at zero relative pressure. On occasion, bubbles can be captured such that when no relative pressure is applied, the bubble height will be greater than zero. For ease of experiment, these microrobots are removed from the workspace, dried, and placed in the workspace again. Optimization of the cavity size to ensure proper bubble capture is left as a future work.

To determine how the applied relative pressure affects the picking force of the microrobot, the height of the bubble must be understood and controlled. When not in contact with a micro-object, the normal distance from the microrobot to the highest point of the bubble is used to measure  $h$ . However,

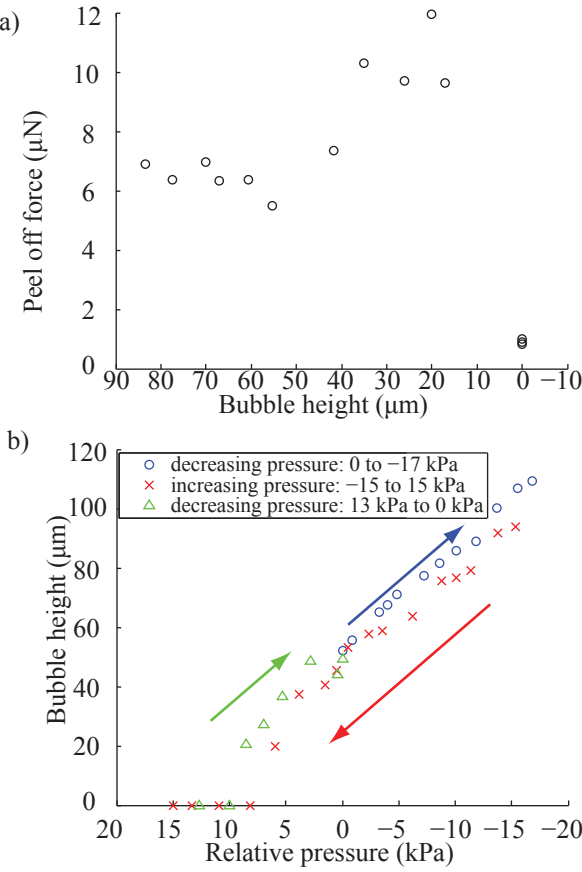


Fig. 7: (a) Detachment magnetic force as a function of bubble height. The height of the bubble is modulated with pressure, with care to keep the volume of the bubble relatively constant. The maximum observed detachment force is 12  $\mu\text{N}$  while the minimum force, when the bubble has been forced into the microrobot cavity, is 0.83  $\mu\text{N}$ , showing a peak switching ratio of 14:1. The minimum peel off force is identical to the force required to peel the microrobot from its side without a bubble. (b) Bubble height as a function of pressure. The hysteresis effect is made negligible by modulating the pressure quickly. The arrows indicate the direction of pressure increasing or decreasing as a function of time, in the order of blue, red, then green. Microrobot magnetization:  $\vec{m} = 0.511 \mu\text{Am}^2$ .

gas from solution can enter or leave the bubble at positive or negative pressures, respectively. This will also manipulate the bubble size over time. Figure 6(b) shows initial experiments to characterize the change of the bubble due to constantly applied relative pressures over 15 minutes. The constant rate of bubble size change is predicted by the literature, as the rate of change in the bubble size becomes approximately constant when

$$t \gtrsim 10 \frac{r_b^2}{\pi D}, \quad (9)$$

where  $r_b$  is the radius of the bubble and  $D$  is the diffusivity of air into water,  $2 \times 10^{-5} \text{ cm}^2/\text{s}$  [21]. For our bubble, this time is on the order of five to ten seconds.

Figure 6(b) demonstrates that at larger relative pressure magnitudes ( $\pm 10 \text{ kPa}$ ), a change in bubble volume will affect the manipulation method, eg: if a large negative relative pressure is applied to the bubble for a large time then the detachment condition,  $h < 0$ , will require a larger positive relative pressure. We then want to avoid working in these regions to maintain control of the bubble volume. These results can be used to control  $h$  such that over time a larger bubble can be obtained to aid initial contact of the object,

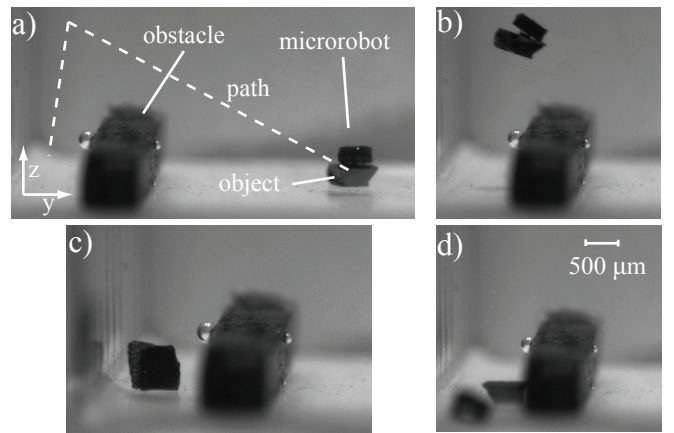


Fig. 8: Frames from the manipulation proof of concept. (a) The microrobot attaches to the silicon part, and (b,c) by applying a magnetic force in the  $yz$ -direction the microrobot is able to move over a barrier splitting the workspace into two regions. (d) The microrobot then separates from the micro-object using a rolling motion once the positive pressure is applied. Video available in supplementary materials.

or  $h$  can be decreased slowly over time to control and place the object.

As the applied relative pressure is given as the control input, the detachment force as a function of pressure, coupled by  $h$ , is investigated. A maximum force of 12  $\mu\text{N}$  and a minimum force of 0.83  $\mu\text{N}$  yield a switching ratio of 14:1 as shown in Fig. 7(a). The bubble height is manipulated with an applied pressure and the force required to peel the microrobot is recorded. To reduce the time dependency of  $h$ , the results from Fig. 6 are considered. For a given negative pressure used to increase  $h$ , a positive pressure equal to the magnitude of the negative pressure is applied after the peel off measurement for approximately an equal amount of time. The maximum detachment force is observed when  $h \rightarrow 0$ . Once the modulated bubble height is such that the bubble could not come into contact with the substrate, the detachment force became minimized and constant.

To demonstrate controllability of the bubble height, Fig. 7(b) shows the bubble height for an applied pressure. To eliminate hysteresis from air diffusion effects, the measurement occurs over a period of five seconds. As confirmation of the lack of diffusion during this experiment, it can be seen in Fig. 7(b) that when the pressure returns to zero, the bubble height returns to its original value.

Experiments have shown that the pressure changes will affect undesired bubbles in the workspace as well. These can cause additional attachment force between the micro-object and the working surface, greatly increasing the required capillary force to lift the object. This adhesion will also resist 2D motion, possibly preventing any actuation of the object.

#### B. 3D Manipulation Experiments

The microrobot's ability to pick-and-place an object in 3D is demonstrated in Fig. 8. The micro-object is a planar silicon chiplet fabricated to roughly the size of the microrobot, 500 x 500  $\mu\text{m}$ . An obstacle, 1 mm thick acrylic, blocks the microrobot from placing the micro-object in the goal region, the camera focal plane on the left side. A bubble is seen captured on the obstacle due to surface defects. The microrobot, with an extended bubble, is rolled on top of

the object. The approximate open loop path is given by the dashed line. The microrobot is pulled in 3D using magnetic forces ( $\vec{F}_m$ ) to overcome the barrier. The microrobot lands on its side, with the microrobot facing the camera. The microrobot uses a rolling locomotion to move into the goal region, and separates from the object. The microrobot then rolls into the foreground of the focal plane.

### C. Scaling

When the microrobot/micro-object system has a zero net velocity in a fluid medium and is not in contact with a surface, it is apparent that the capillary force must be greater than the effective weight of the micro-object, and the magnetic force must be greater than the effective weight of both the micro-object and microrobot. When considering the maximum capillary force, examining eqs. (3,4) show  $r$  should be maximized and  $R$  should be minimized, though a greater importance is placed on maximizing  $r$  as  $F_c \propto r^2$  and  $F_c \propto R^{-1}$ . This also indicates scaling of this technique is favorable for microrobots as  $F_c \propto L^1$ . These conditions can be obtained by manipulating the bubble to have a short distance between the microrobot and object and a large contact radius. For a microrobot of a fixed size, this is facilitated by a larger cavity to magnetic volume ratio in order to accommodate a large air bubble. The magnetic force scales with  $L^3$ , so the loss of magnetic volume is detrimental to the ability to manipulate objects. However, the maximum capillary force must be greater than the effective weight of the micro-object; thus the optimal design will be dependent on the specific application.

## VI. CONCLUSIONS

In this work, we have shown the initial investigation of a capillary gripper for an untethered mobile magnetic microrobot. A small bubble is captured in a cavity molded into the microrobot. The bubble volume is modulated by an external relative pressure on the microrobot workspace. The bubble attaches to micro-objects by capillary force, and retraction of the bubble is used to detach the micro-object from the microrobot. The current system and microrobots yield a maximum switching ratio of 14:1. This manipulation method would be useful for 3D transport and assembly of microparts in enclosed microfluidic devices where external pressure is a controlled parameter.

Placement of the object is currently accomplished by using 2D rolling actuation to position the object before release. This introduces inaccuracies in placement and could possibly damage the object as it comes into contact with the surface. Future work will focus on precision manipulation and placement of objects in arbitrary 3D environments. It is envisioned this method could build 3D MEMS devices or tissue-engineered structures [6].

Microrobots of dimensions  $500 \times 500 \times 100 \mu\text{m}$  with cavities of  $100 \mu\text{m}$  radius are investigated in this work. Future work entails investigating the optimization of a microrobot for a specific task. Other detachment mechanisms could be developed to cause the bubble to detach from the micro-object without the bubble fully retracting. While

planar micro-objects and substrates have been investigated, the method could be generalized to non-planar objects.

## REFERENCES

- [1] B. R. Donald, C. G. Levey, C. D. McGraw, I. Paprotny, and D. Rus, "An untethered, electrostatic, globally controllable mems micro-robot," *Journal of Microelectromechanical Systems*, vol. 15, no. 1, pp. 1–15, 2006.
- [2] D. R. Frutiger, K. Vollmers, B. E. Kratochvil, and B. J. Nelson, "Small, fast, and under control: Wireless resonant magnetic micro-agents," *International Journal of Robotics Research*, vol. 29, no. 5, pp. 613–636, 2009.
- [3] O. Sul, M. Falvo, R. Taylor, S. Washburn, and R. Superfine, "Thermally actuated untethered impact-driven locomotive microdevices," *Applied Physics Letters*, vol. 89, p. 203512, 2006.
- [4] S. Martel, M. Mohammadi, O. Felfoul, Z. Lu, and P. Pouponneau, "Flagellated magnetotactic bacteria as controlled MRI-trackable propulsion and steering systems for medical nanorobots operating in the human microvasculature," *International Journal of Robotics Research*, vol. 28, no. 571–582, 2009.
- [5] B. Behkam and M. Sitti, "Bacterial flagella-based propulsion and on/off motion control of microscale objects," *Applied Physics Letters*, vol. 90, p. 023902, 2007.
- [6] S. Tasoglu, E. Diller, S. Guven, M. Sitti, and U. Demirci, "Untethered micro-robotic coding of three-dimensional material composition," *Nature Communications*, vol. 5, no. 3124, DOI: 10.1038/ncomms4124, 2014.
- [7] E. Diller, J. Giltinan, and M. Sitti, "Independent control of multiple magnetic microrobots in three dimensions," *International Journal of Robotics Research*, vol. 32, no. 5, pp. 614–631, 2013.
- [8] C. Pawashe, S. Floyd, E. Diller, and M. Sitti, "Two-dimensional autonomous microparticle manipulation strategies for magnetic microrobots in fluidic environments," *IEEE Transactions on Robotics*, vol. 28, no. 2, pp. 467–477, 2012.
- [9] Z. Ye, E. Diller, and M. Sitti, "Micro-manipulation using rotational fluid flows induced by remote magnetic micro-manipulators," *Journal of Applied Physics*, vol. 112, no. 6, p. 064912, 2012.
- [10] W. Hu, K. S. Ishii, and A. T. Ohta, "Micro-assembly using optically controlled bubble microrobots," *Applied Physics Letters*, vol. 99, no. 9, pp. 094103–094103, 2011.
- [11] S. Tottori, L. Zhang, F. Qiu, K. K. Krawczyk, A. Franco-Obregón, and B. J. Nelson, "Magnetic helical micromachines: fabrication, controlled swimming, and cargo transport," *Advanced Materials*, vol. 24, no. 6, pp. 811–6, 2012.
- [12] J. O. Kwon, J. S. Yang, and S. Chung, "Untethered microrobot actuated by an electromagnetic field with an acoustically oscillating bubble for bio/micro-object manipulation," in *Solid-State Sensors, Actuators and Microsystems Conference*, pp. 282–285, 2011.
- [13] D. O. Popa and H. E. Stephanou, "Micro and mesoscale robotic assembly," *Journal of Manufacturing Processes*, vol. 6, no. 1, pp. 52–71, 2004.
- [14] B. López-Walle, M. Gauthier, and N. Chaillet, "Principle of a submerged freeze gripper for microassembly," *IEEE Transactions on Robotics*, vol. 24, no. 4, pp. 897–902, 2008.
- [15] P. Lambert, *Capillary forces in microassembly: modeling, simulation, experiments, and case study*. Springer, 2007.
- [16] A. A. Atchley and A. Prosperetti, "The crevice model of bubble nucleation," *Journal of the Acoustical Society of America*, vol. 86, p. 1065, 1989.
- [17] M. Kummer, J. Abbott, B. Kratochvil, R. Borer, A. Sengul, and B. Nelson, "Octomag: An electromagnetic system for 5-DOF wireless micromanipulation," *IEEE Transactions on Robotics*, vol. 26, no. 6, pp. 1006–1017, 2010.
- [18] P. Attard and S. J. Miklavcic, "Effective spring constant of bubbles and droplets," *Langmuir*, vol. 17, no. 26, pp. 8217–8223, 2001.
- [19] E. Diller, C. Pawashe, S. Floyd, and M. Sitti, "Assembly and disassembly of magnetic mobile micro-robots towards deterministic 2-D reconfigurable micro-systems," *International Journal of Robotics Research*, vol. 30, no. 14, pp. 1667–1680, 2011.
- [20] M. Imbabi, K. Jiang, and I. Chang, "Net shape fabrication of stainless-steel micro machine components from metallic powder," *Journal of Micromechanics and Microengineering*, vol. 18, no. 11, p. 115018, 2008.
- [21] P. Epstein and M. Plesset, "On the stability of gas bubbles in liquid-gas solutions," *Journal of Chemical Physics*, vol. 18, p. 1505, 1950.